INTER-NOISE 2006
3-6 DECEMBER 2006
HONOLULU, HAWAII, USA

On the development of an efficient parallel hybrid solver with application to acoustically treated aero-engine nacelles

Willie R. Watson
NASA Langley Research Center
Mail Stop 128
Hampton, VA 23681 USA

Douglas M. Nark
NASA Langley Research Center
Mail Stop 463
Hampton, VA 23681 USA

Duc T. Nguyen
Old Dominion University
135 Kaufman Hall
Norfolk, VA 23529, USA

Siroj Tungkahotara
Old Dominion University
135 Kaufman Hall
Norfolk, VA 23529, USA

ABSTRACT

A finite element solution to the convected Helmholtz equation in a nonuniform flow is used to model the noise field within 3-D acoustically treated aero-engine nacelles. Options to select linear or cubic Hermite polynomial basis functions and isoparametric elements are included. However, the key feature of the method is a domain decomposition procedure that is based upon the intermixing of an iterative and a direct solve strategy for solving the discrete finite element equations. This procedure is optimized to take full advantage of sparsity and exploit the increased memory and parallel processing capability of modern computer architectures. Example computations are presented for the Langley Flow Impedance Test Facility and a rectangular mapping of a full scale, generic aero-engine nacelle. The accuracy and parallel performance of this new solver are tested on both model problems using a supercomputer that contains hundreds of central processing units. Results show that the method gives extremely accurate attenuation predictions, achieves super-linear speedup over hundreds of CPUs, and solves upward of 25 million complex equations in a quarter of an hour.

1 NOMENCLATURE

$c_0, \rho_0, \vec{u}_0$	= sound speed, mean density, mean velocity vector
F, Φ	= vector containing source effects, vector of nodal velocity potentials
f, i, N	= source frequency, unit imaginary number, order of global stiffness matrix
$I, PP, \Delta dB$	= acoustic intensity, acoustic power, liner attenuation
K, ζ_E	= stiffness matrix, dimensionless node impedance matrix
$\vec{n}, \vec{\nabla}$	= unit normal vector, 3-D gradient operator
$p, \phi, \vec{u}$	= acoustic pressure, velocity potential, particle velocity vector
ζ	= wall impedance normalized by $\rho_0 c_0$
P_E, U_E	= vectors for defining nonreflecting boundary condition
$\Re, *, \bullet$	= real part of complex expression, complex conjugate, dot product
S_1, S_3	= source boundary, exit boundary

Subscripts:

I, B, s = interior unknown, boundary unknown, source potential

2 INTRODUCTION

The reduction of commercial aircraft noise in communities near airports has become a major socio-economic problem both within the U.S. and abroad. Because of the continuous increase in aircraft capacity and the number of flights, commercial air transportation remains in continuous growth. However, the high noise levels emitted during takeoff and landing threaten to severely compromise the growth of commercial air transportation systems worldwide. Thus, the reduction of aircraft noise especially in communities near airports has become a major challenge. High levels of noise produced by modern aircraft at take-off and landing may be categorized as either airframe or engine noise. Airframe noise is due to the interactions of the flow with the solid aircraft components. Engine noise is generally decomposed into its constitutive sources, two main components being jet and fan noise. The jet noise is caused by the ejection of fast hot gases through the engine and fan noise is fluid/structure interaction noise generated by the rotating turbomachinery within the engine. The introduction of high-bypass ratio engines has enabled a substantial reduction of jet noise so that engine noise in today's large civil aircraft is dominated by fan noise [1].

Noise reduction methods for fan noise have mainly involved the installation of advanced nacelle liners within the nacelles to absorb the noise generated by the fan noise sources [2]. This approach requires an accurate prediction of both the noise absorbed and radiated from modern nacelles so that the treatment can be optimized for maximum noise reduction. Due to the complex 3-D geometries and flows inside modern nacelles, such predictions remain out-of-reach of theoretical modeling and experimental methods have proved too costly. Thus, the tool of choice has been numerical simulation. To this end, several 3-D finite element codes have been developed both in the U.S. and abroad [3, 4]. These codes generate a large, sparse, linear system of algebraic equations that must be solved in an efficient manner to compute the radiated noise and provide the ability to assess various low-noise designs.

Methods for solving large sparse systems of linear algebraic equations are either direct or iterative. Iterative methods in use today are usually based upon Krylov subspace methods [5]. The iterative methods have the advantage of not requiring computation and storage of an inverse matrix and are highly scalable on massively parallel supercomputers. However, the convergence rates of the iterative methods are highly dependent on the existence of good preconditioners that are currently not available for nacelle problems with arbitrary 3-D geometries and wall lining. Consequently, the more robust direct methods have generally been the solvers of choice in nacelle aeroacoustics [3, 4]. Because direct methods are based upon the factorization and storage of a matrix inverse, they are inefficient when used on realistic 3-D geometries.

In an earlier paper, the authors introduced a "hybrid" solve strategy for analyzing acoustic fields in aero-engine ducts [6]. This approach has the potential to overcome many of the limitations of iterative and direct methods. However, the work in the earlier paper contained several shortcomings. First, it was tested only in a hard wall duct and at a single frequency. Second, the earlier work was restricted to symmetric matrices so that mean flow could not be accommodated. Third, the developed software was limited to a million equations and to only 64 central processing units (CPUs). Finally, the analysis was restricted to a uniform brick element with linear basis functions that limited its applicability to a rectangular geometry. The purpose of this paper is to describe efforts to remove the above-mentioned limitations of the earlier work.

3 GOVERNING EQUATIONS AND BOUNDARY CONDITIONS

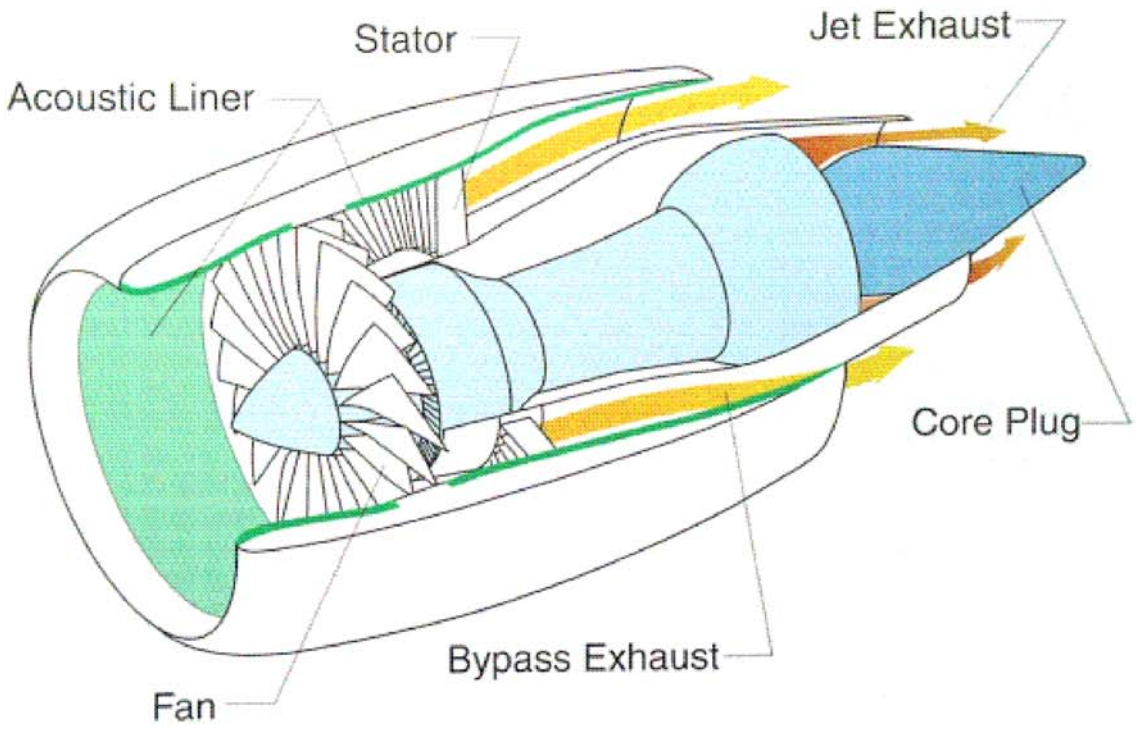

Fig 1: Typical aircraft nacelle with acoustic liners.

Figure 1 is a schematic of an aircraft nacelle with sound absorbing material (acoustic liners). The sound absorbing material is locally reacting and is characterized by an impedance, ζ, that is a function of position along the treated surfaces. The problem at hand is to determine the attenuation produced by the wall lining in the presence of a flowing fluid in the duct. The governing differential equation (assuming irrotational homentropic flow) is [4]

$$-\frac{D}{Dt}\left(\frac{\rho_0}{c_0^2}\frac{D\phi}{Dt}\right)+\vec{\nabla}\bullet(\rho_0\vec{\nabla}\phi)=0,\quad \frac{D}{Dt}=\frac{2i\pi f}{c_0}+\vec{u}_0\bullet\vec{\nabla} \tag{1}$$

Near the fan face, the acoustic velocity potential is assumed known

$$\phi=\phi_s \tag{2}$$

The wall liner boundary condition is expressed in the form [7]

$$\vec{\nabla}\phi\bullet\vec{n}=\frac{\rho_0}{\zeta}\frac{D\phi}{Dt}+\frac{1}{i2\pi f}\left[\vec{u}_0\bullet\vec{\nabla}\right]\left(\frac{\rho_0}{\zeta}\frac{D\phi}{Dt}\right)-\left(\frac{\rho_0}{i2\pi f\zeta}\frac{D\phi}{Dt}\right)\left[\vec{n}\bullet\left(\vec{n}\bullet\vec{\nabla}\vec{u}_0\right)\right] \tag{3}$$

At the exit of the nacelle a nonlocal, nonreflecting boundary condition [8] that has been extended by the authors to include flow effects is implemented

$$P_E=\zeta_E U_E \tag{4}$$

Finally, at the intersections between hard and treated surfaces the acoustic pressure and normal component of acoustic particle velocity are required to be continuous.

Upon obtaining the acoustic velocity potential, the acoustic particle velocity vector and acoustic pressure field are post-processed from the irrotationality and the linearized, homentropic, conditions

$$\vec{u} = \vec{\nabla}\phi, \qquad p = -\rho_0 \frac{D\phi}{Dt} \tag{5}$$

The sound attenuated by the wall lining in decibels is obtained from the log of the ratio of the input to the output acoustic power

$$\Delta dB = 10\log_{10}\left[\frac{PP(S1)}{PP(S3)}\right], \qquad PP(S) = \int_S I dS \tag{6}$$

where the acoustic intensity, I, is expressed in the form given by Morfey [9]

$$I = \frac{1}{2}\Re\left[p\vec{u^*}\bullet\vec{n} + \rho_0(\vec{u}_0\bullet\vec{u})(\vec{u^*}\bullet\vec{n}) + \frac{pp^*}{\rho_0 c_0^2}(\vec{u}_0\bullet\vec{n}) + \frac{p^*}{c_0^2}(\vec{u}_0\bullet\vec{u})(\vec{u}_0\bullet\vec{n})\right] \tag{7}$$

4 THE FINITE ELEMENT MODEL

The numerical method chosen to solve the potential equation coupled with the sound source, wall impedance, and exit boundary conditions is the finite element method (FEM). Details of the FEM are beyond the scope of the current paper. However, a brick element containing either linear or cubic Hermite polynomial basis functions is utilized to obtain the solution for the acoustic potential within the nacelle. For nonuniform geometries the brick element is transformed to an isoparametric element. Galerkin's finite-element method is used to minimize the field error and obtain the acoustic velocity potential. A weak formulation is introduced so that the wall and exit impedance boundary conditions are introduced at the element level. The elements for the entire domain are assembled in the usual manner and the source condition is satisfied by constraining the nodal degrees of freedom at the source plane. This leads to a sparse system containing N complex, linear, algebraic equations of the form

$$K\Phi = F \tag{8}$$

5 THE HYBRID EQUATION SOLVER

The equation solving paradigm introduced in this text is based upon the intermixing of a direct sparse solver and an iterative solver. The key idea is to combine the benefits of direct sparse solvers (robustness and speed) and iterative solvers (low memory usage and scalability) to obtain the solution to Eq. (8) in a memory and time efficient manner. The hybrid solve strategy begins by partitioning Eq. (8) into interior and boundary unknowns [11]

$$\begin{array}{rcrcl} K_{BB}\Phi_B & + & K_{BI}\Phi_I & = & F_B \\ K_{IB}\Phi_B & + & K_{II}\Phi_I & = & F_I \end{array} \tag{9}$$

Solutions to Eq. (9) are of the form

$$\begin{array}{rcl} \overline{K}_{BB}\Phi_B & = & \overline{F}_B \\ K_{II}\Phi_I & = & F_I - K_{IB}\Phi_B \end{array} \tag{10}$$

where

$$\begin{aligned} \overline{K}_{BB} &= K_{BB} - K_{BI}K_{II}^{-1}K_{IB} \\ \overline{F}_B &= F_B - K_{BI}\overline{F}_I \\ K_{II}\overline{F}_I &= F_I \end{aligned} \tag{11}$$

The sequence of steps constituting the hybrid DD formulation proposed in this text are

1. Compute $K_{IB}, K_{BI}, K_{II}, K_{BB}, F_B$, and F_I using efficient sparse assembly algorithms [10]
2. Factorize the sparse matrix K_{II} and compute $\overline{F}_I$ from Eqs. (11) using algorithms and software discussed in [10].
3. Compute $\overline{K}_{BB}$ and $\overline{F}_B$ using Eqs. (11). Explicit computation of $\overline{K}_{BB}$ will be expensive due to the need to perform the triple product in Eq. (11)
4. Use an iterative solver to obtain the boundary unknowns in Eq. (10) and avoid the computation of this triple product.
5. Upon obtaining the boundary unknowns the interior unknowns are obtained from Eq. (10) by using the previously factorized sparse matrix K_{II}
6. To better facilitate application of the strategy on massively parallel computer architectures, a domain decomposition (DD) formulation [12, 13] is applied to the computational volume. Equations (10)-(11) are therefore subdivided into subdomains and each subdomain assigned to a processor. After each processor has completed its task, the solutions are merged to obtain the solution vector. The solution vector is then post-processed to obtain the sound attenuation, ΔdB.

6 RESULTS AND DISCUSSIONS

This section presents results for zero flow, as well as selected examples with flow. The hybrid solver uses sparse factorization techniques presented in the book of Nguyen [10] and implements either the conjugate gradient (symmetric matrices) or the Generalized Minimal Residual (asymmetric matrices) as the iterative solver [5] for the dense system defined in Eq. (10). Both iterative solvers are implemented with the diagonals of K_{BB} as the preconditioner. Therefore a less expensive preconditioner than that provided by the Jacobi preconditioner has been implemented. The primary hardware utilized was the Columbia cluster (a Silicon Graphics Altix 3700 distributed memory system with 1 TB of RAM and 512 Itanium2 CPUs with clock speeds of 1.5 GHz). The developed software is referred to as the direct iterative parallel sparse solver (DIPSS). The authors have examined a number of freely available and at least two commercially available parallel, sparse, direct solvers against which to benchmark the speed of the new hybrid solve strategy. It was determined that the commercially available SGI parallel sparse solver has a lower wall clock time than the other solvers on the Columbia clusters. Thus, the decision was made to benchmark the hybrid solver against the SGI parallel, direct, sparse solver. It should be noted that the lower wall clock time of the SGI sparse solver may reflect the fact that this solver was specifically designed to take full advantage of many special features of Columbia's hardware. Further, some of the commercially available software packages were limited to only 32 CPUs. Our comparison study with

other direct solvers was restricted therefore to only 32 CPUs. It should also be noted that many of the solvers tested were limited in the number of reordering schemes.

Two rectangular geometries are used to benchmark the accuracy, efficiency, and robustness of the DIPSS solution methodology presented in this paper. The first geometry is that of the LaRC Flow Impedance Test Facility and the second geometry is a rectangular mapping of a generic aero-engine duct. The Langley Flow Impedance Test Facility geometry was chosen because it affords the authors the opportunity to compare solution statistics to that of the SGI parallel sparse solver and with the version of the DIPSS solver presented in an earlier paper [6]. The generic aero-engine duct was chosen because it allows for large-scale computations in geometries with short length to diameter ratios (comparable to that of a large commercial engine) where many modes are propagating and tens of millions of grid point are required for accurate resolution of the sound field. Only uniform rectangular elements are implemented due to the rectangular geometries involved. Furthermore, the iterative solve portion of the DIPSS software was run until the L2 norm of the residual reached a specified tolerance or until 2,000 iterations were reached. The tolerance was set at 10^{-8} for all results presented in this section.

6.1 LaRC Flow Impedance Test Facility

This geometry is 81.28 cm long and contains a 5.08 cm $\times$ 5.08 cm cross section. We consider zero flow ($M_0 = 0.0$) and a $36\times36\times775$ uniform grid ($N = 1,004,440$). Hard wall statistics for the SGI sparse solver are compared to that of an earlier version (DIPSS V1) and to the current version (DIPSS V2) of the DIPSS software in table 1. Standard atmospheric conditions (ρ_0=1.2 kg-m^{-3} and c_0=344 m/s) were used to perform the computations.

Table 1: Hard Wall Statistics for LaRC Flow Impedance Test Facility.
(Zero flow, hard walls, f=3.5 kHz, $N = 1,004,440$)

	Wall Clock Time, sec			RAM Memory, GB	
CPUs	SGI	DIPSS V1	DIPSS V2	SGI	DIPSS V2
1	1428	N/A	N/A	12.01	N/A
2	751	4880	N/A	12.01	N/A
4	400	1766	N/A	12.01	N/A
8	242	432	402	12.02	11.04
16	377	146	133	12.09	9.19
32	150	60	55	12.66	6.89
64	185	33	35	12.29	10.62
128	192	89	70	13.00	12.76
256	580	155	146	13.00	12.86

Table 1 exemplifies the primary problem encountered by direct solvers (such as the SGI solver) for even moderate size acoustic problems. The SGI solver (column 2) leads to low wall clock turnaround times for a small number of CPUs, but scales poorly as the number of CPUs is increased. DIPSS (columns 3 and 4) gives super-linear speedup over 64 CPUs and is considerably faster than the SGI solver on 128 and 256 CPUs. Notice that the wall clock time for DIPSS is considerably less than the direct solver on as little as 16 CPUs. DIPSS gives a reduction of a factor of six in wall clock turnaround compared to the SGI solver on 64 CPUs. Observe also that more

than four CPUs are required to obtain a solution using the current strategy, whereas, for the earlier version this same example could be solved on as little as two CPUs. Thus, the current implementation of DIPSS (DIPSS V2) requires more startup memory, but runs a little more efficiently than the earlier version (DIPSS V1). The corresponding RAM for the SGI solver and DIPSS V2 are given in columns 5 and 6, respectively. Note that DIPSS gives savings also in the RAM memory compared with the SGI solver. RAM memory savings are observed to be considerable in the middle of the CPU range.

Table 2: Attenuations and Solver Statistics for LaRC Flow Impedance Test Facility. (Zero flow, $N = 1,004,440$, 16 CPUs used)

	Hard Wall Statistics				Soft wall duct statistics			
f kHz	Anal ΔdB	DIPSS ΔdB	Wall Clock	No. Iter	Anal ΔdB	DIPSS ΔdB	Wall Clock	No. Iter
0.5	0.00	0.00	147	57	34.75	34.71	154	79
1.0	0.00	0.00	144	55	41.96	41.90	153	77
1.5	0.00	0.00	145	51	45.65	45.58	152	75
2.0	0.00	0.00	145	51	47.60	47.53	151	72
2.5	0.00	0.00	140	38	48.13	48.05	149	67
3.0	0.00	0.00	135	26	47.19	47.11	148	63
3.5	0.00	0.00	130	15	44.62	44.55	142	48
4.0	0.00	0.00	134	23	40.46	40.38	143	50
4.5	0.00	0.00	141	41	35.20	35.13	145	58
5.0	0.00	0.00	137	31	29.76	29.70	159	72

To validate solution accuracy of the DIPSS solution over a frequency range, the authors used the analytically computed attenuation produced by the liner, ΔdB, as a metric. This metric is physically more meaningful than the acoustic potential because the human ear perceives it as the noise source propagates down the duct. In addition, the difference between the analytical and numerical values provides some metric for the assessment of error in the calculations. Attenuations computed from the DIPSS V2 solution vectors are compared to the analytical values for a frequency range of 0.5 to 5.0 kHz in table 2. In addition, the wall clock time in seconds and the number of iteration required for the iterative solver to converge is also presented. Here, the hard wall duct has a planar wave source, the soft wall duct uses the lowest order mode as the sound source, and the liner is 81.28 cm in length and has a uniform impedance of ζ=1.5 -0.5i. The impedance of the upper and two sidewalls are set to rigid wall values. As expected, no attenuation of the sound is obtained in the rigid wall duct (table 2) due to the absence of the wall treatment. The DIPSS attenuations for the hard wall duct are in exact agreement with the analytical values of zero. Note that the presence of the liner leads to an attenuation of the sound and that the frequency of peak attenuation is 2.5 kHz. Attenuations computed from the DIPSS V2 solution vector are in excellent agreement with the analytical value in the lined duct. When compared to the wall clock time without lining, the effects of the wall lining are to increase the wall clock time only slightly. Just as in the rigid wall duct, the wall clock times that are required for a converged solution are nearly constant across the frequency range.

Table 3 compares the analytical attenuation with that obtained using the solution vector from

Table 3: Attenuations for LaRC Flow Impedance Test Facility at Mach 0.45.
(Soft wall, cubic Hermite element, $N = 595,968$, 8 CPUs used)

f kHz	Anal ΔdB	SGI ΔdB
0.5	13.06	13.01
1.0	17.24	17.18
1.5	19.33	19.26
2.0	20.67	20.59
2.5	21.62	21.54
3.0	22.33	22.26
3.5	22.87	22.79
4.0	23.24	23.16
4.5	23.45	23.39
5.0	23.53	23.46

the SGI solver for a flow Mach number of 0.45 in the soft wall duct. Here, the 3-D cubic Hermite element is used with a $16\times16\times291$ uniformly spaced grid. This grid is considerably coarser than that used with the linear element in table 2. However, with the higher order cubic element the SGI attenuations are still in excellent agreement with the analytical values.

6.2 Generic Aero-Engine Duct

The generic aero-engine duct is modeled as a rectangular duct by cutting it along the axis and unwrapping it into a rectangular geometry. When unwrapped, the nacelle engine duct has a 317.5 cm $\times$ 63.5 cm rectangular cross-section and is 219.5 cm in length. Thus, the volume of our generic aero-engine duct is slightly more than 2,075 times that of the Flow Impedance Test Facility investigated in the previous example, and requires many more grid points for accurate resolution of the acoustic field. The highest frequency of interest (5.0 kHz) is roughly equivalent to four to six times the blade passage frequency (BPF) for a typical large commercial engine. Just to illustrate the capability of the hybrid solver we have used a $100\times100\times2501$ uniformly spaced grid ($N = 25,010,000$). Such a large number of points are far beyond what can be solved using direct sparse solvers such as the SGI solver.

Table 4 compares the analytical and DIPSS attenuations and gives solver statistics for the generic aero-engine duct. All parameters are identical to those of table 2 with the exception of the duct dimensions and the grid. Speedup studies were conducted on the generic aero-engine duct but because of space limitations these results could not be presented. However, super-linear speedup was observed on as many as 256 CPUs and this speedup drops to linear on 384 CPUs. Results in table 4 were run in parallel on 192 CPUs and required slightly more than 333 GB of RAM. Hard wall attenuations in the generic aero-engine duct are in excellent agreement with the analytical values of zero over the full range of source frequencies. It is observed that in this larger, more realistic volume, the wall clock turnaround and the number of iterations required to obtain a converged solution in the hard wall duct are essentially constant across the full range of source frequencies. A more interesting set of results is obtained in the soft wall duct. Note that the chosen lining is not very effective at attenuating the sound and the wall clock times are considerably higher than the rigid wall case. The predicted soft wall attenuations are in excellent agreement with the

Table 4: Attenuations and Solver Statistics for Generic Aero-Engine Duct.
(Zero flow, $N = 25,010,000$, 192 CPUs used)

	Hard Wall Statistics				Soft wall duct statistics			
f kHz	Anal ΔdB	DIPSS ΔdB	Wall Clock	No. Iter	Anal ΔdB	DIPSS ΔdB	Wall Clock	No. Iter
0.5	0.000	0.000	1048	208	4.073	4.071	1695	427
1.0	0.000	0.000	1089	218	0.920	0.920	1933	498
1.5	0.000	0.000	1060	209	0.393	0.393	1921	492
2.0	0.000	0.000	1060	209	0.217	0.217	1928	494
2.5	0.000	0.000	1060	210	0.137	0.137	2105	537
3.0	0.000	0.000	1059	210	0.094	0.094	3491	985
3.5	0.000	0.000	1045	211	0.069	0.069	6810	2,000
4.0	0.000	0.000	1027	211	0.053	0.052	7047	2,000
4.5	0.000	0.000	1035	212	0.041	-0.275	6829	2,000
5.0	0.000	0.000	1016	213	0.033	1.139	6841	2,000

analytical attenuations up to about 4.0 kHz. However, beyond 4.0 kHz the solution vector in the soft wall duct had not converged within the 2,000 iteration limit and the predicted attenuations are poor. This suggests that a better preconditioner is required for frequencies that are larger than 4.0 kHz in the soft wall duct.

6.2 CONCLUSIONS

The results of this study may be summarized as follows:

1. When compared to analytical solutions, the hybrid solve strategy gives extremely accurate attenuation predictions in rigid and soft wall ducts for the range of frequencies of interest in full-scale aero-engine nacelles. This accuracy can be obtained using a preconditioner less expensive than that provided by the Jacobi preconditioner.

2. In contrast to direct solve strategies, the hybrid solve strategy gives super-linear speedup over hundreds of processors and allows for upward of 25 million complex unknowns to be solve in slightly more than a quarter of an hour.

3. In addition to significant increases in speedup compared to the commonly used direct sparse solver, the hybrid solve philosophy leads to significant reduction in RAM memory.

4. Results of this study show that for full-scale aero-engine modeling in lined ducts, that the hybrid solver convergence rate is slow for source frequencies above 4.0 kHz. Thus, an improved preconditioner appears needed for noise computations beyond this source frequency.

The above conclusions are based upon the use of a rectangular geometry for which exact analytical solutions are available for comparison. A similar study involving nonuniform geometry and nonuniform mean flow for which exact solutions are not available is currently underway.

References

[1] E. Envia," Fan Noise Reduction: An Overview," AIAA Paper 2001-0661, *Proceedings of the 7th AIAA/CEAS Aeroacoustics Conference & Exhibit*, Maastricht, The Netherlands, May 28 – 30, 2001.

[2] G. W. Bielak, J. W. Premo, and A. S. Hersh,"Advanced Turbofan Duct Liner Concepts," *NASA/CR-1999-209002*, Feb. 1999.

[3] D. Nark, W. Watson, and M. Jones, "Further Investigation of Two Acoustic Propagation Codes for Three-Dimensional Geometries" AIAA Paper 2006-2586, *Proceedings of the 12th AIAA/CEAS Aeroacoustics Conference & Exhibit*, Cambridge, Massachusetts, USA, May 8 – 10, 2006.

[4] Free-Field-Technologies-S.A. Actran 2006 Aeroacoustic Solutions, "Actran/TM and Actran/LA - User's Manual." 16, place de l'Universite, 1348 Louvain-la-Neuve, Belgium, 2006.

[5] Y. Saad,*Iterative Methods for Sparse Linear Systems*, Society for Industrial and Applied Mathematics, Second Edition, 3600 University City Science Center, Philadelphia PA, 2003.

[6] D. T. Nguyen, W. R. Watson, S. Tungkahotara, and S. D. Rajan, "Parallel Finite Element Domain Decomposition for Structural/Acoustic Analysis, "Journal of Computational and Applied Mechanics," Vol. 4., No. 2, pp. 189-201, April 2003.

[7] M. K. Myers, "On The Acoustic Boundary Condition In The Presence Of Flow," *Journal Of Sound And Vibrations*, Vol. 71, No. 3, 1980, pp. 429-434.

[8] W. E. Zorumski, W. R. Watson, and S. L. Hodge, "A Nonlocal Computational Boundary Condition for Duct Acoustics," *Journal of Computational Acoustics*, Vol. 3, No.1, June 1995, pp. 15-26.

[9] C. L. Morfey, "Acoustic Energy in Non-uniform Flows," *Journal of Sound and Vibration*, Vol. 14, 1971, pp. 159-170.

[10] D. T. Nguyen, *Parallel-Vector Equation Solver For Finite Element Engineering Applications*, Kluwer Academic/Plenum Publishers, 233 Spring Street, New York, NY, 2002.

[11] D. Gute, "Solving large, sparse matrix equations using Multi-Level Substructuring techniques on parallel processor networks," AIAA Paper 92-4380, *AIAA/USAF/NASA/OAI Symposium on Multidisciplinary Analysis and Optimization, 4th*, Cleveland, OH, Sept. 21-23, 1992, pp. 1078-1088.

[12] M. A. Moayyad and D. T. Nguyen, "An algorithm for domain decomposition in finite element analysis," *Journal of Computers and Structures*, Vol 39, No. 1–4, 1991, pp. 277-290.

[13] G. Karypis and V. Kumar, "METIS: Unstructured Graph Partitioning and Sparse Matrix Ordering," Version 2.0, University of Minnesota, 1995.